Modeling Current Transport in Carbon Nanotube Transistors

(Invited Paper)

Mahdi Pourfath and Siegfried Selberherr
Institute for Microelectronics, TU Wien, 1040 Vienna, Austria
Email: {pourfath|selberherr}@iue.tuwien.ac.at

***Abstract*— Carbon nanotubes (CNTs) have been studied in recent years due to their exceptional electronic, opto-electronic, and mechanical properties. To explore the physics of carbon nanotube field-effect transistors (CNT-FETs) self-consistent quantum mechanical simulations have been performed. Both the electron-photon and electron-phonon interactions in CNT-FETs have been analyzed numerically, employing the non-equilibrium Green's function formalism. The numerical challenges for the analysis of carbon nanotube based photo-detectors have been investigated. The results indicate the non-locality of electron-photon interaction. For accurate analysis it is essential to include many off-diagonals of the electron-photon self-energy. Electron-phonon interaction parameters, such as electron-phonon coupling strength and phonon energy, strongly depend on the chirality and the diameter of the carbon nanotube. The steady-state and the dynamic response of carbon nanotube based transistors have been studied for a wide range of electron-phonon interaction parameters.**

I. Introduction

Novel structures and materials such as multiple gate MOSFETs, carbon nanotube field-effect transistors (CNT-FETs), and molecular based transistors, are expected to be introduced to meet the requirements for scaling. CNTs can be considered as a graphene sheet wrapped into a tube. The way the graphene sheet is wrapped is represented by a pair of indices (n, m) called the chiral vector. The integers n and m denote the number of unit vectors along two directions in the honeycomb crystal lattice of graphene. If $m = 0$, the CNT is called *zigzag*. If $n = m$, the CNT is called *armchair*. Otherwise, it is called *chiral*. CNTs with $n - m = 3$ are metals, otherwise they are semiconductors [1]. Semiconducting CNTs can be used as channels for transistors [2], and metallic CNTs can serve as interconnect wires [3].

CNT-FETs have been considered in recent years as potential alternatives to CMOS devices due to their excellent electronic properties [4, 5]. Some of the interesting electronic properties of CNTs are quasi-ballistic carrier transport [6], suppression of short-channel effects due to one-dimensional electron transport [7, 8], and a nearly symmetric structure of the conduction and the valence band [9], which is advantageous for complementary circuits. Moreover, owing to excellent optical properties of CNTs, all-CNT electronic and opto-electronic devices can be envisioned. The direct band-gap and the tunability of the band-gap with the CNT diameter renders them as suitable candidates for opto-electronic devices, especially for infra-red (IR) applications [10, 11] due to the relatively narrow band gap.

The non-equilibrium Green's function (NEGF) method has been successfully utilized to investigate the characteristics of nano-scale silicon transistors [12], CNT-FETs [13–17], and molecular devices [18–20]. In this work we discuss the NEGF formalism to study quantum transport in CNT-FETs.

The outline of the paper is as follows. In Section II, the NEGF formalism is briefly described. The implementation of this method for CNT-FETs is presented in Section III. In Section IV the electron-photon interaction and photo response of CNT-FETs are investigated. In Section V the device response is studied for a wide range of electron-phonon interaction parameters. After a brief discussion in Section VI conclusions are presented in Section VII.

II. Non-equilibrium Green's Function Formalism

The NEGF formalism initiated by Schwinger, Kadanoff, and Baym [21] allows to study the time evolution of a many-particle quantum system. Knowing the single-particle Green's functions of a given system, one may evaluate single-particle quantities such as carrier density and current. The many-particle information about the system is cast into self-energies, which are part of the equations of motion for the Green's functions. A perturbation expansion of the Green's functions is the key to approximate the self-energies. Green's functions enable a powerful technique to evaluate the properties of a many-body system both in thermodynamic equilibrium and non-equilibrium situations.

Four types of Green's functions are defined as the non-equilibrium statistical ensemble averages of the single particle correlation operator [22]. The greater Green's function $G^{>}$ and the lesser Green's function $G^{<}$ deal with the statistics of carriers. The retarded Green's function G^{R} and the advanced Green's function G^{A} describe the dynamics of carriers.

$$\begin{aligned} G^{>}(1,2) &= -i\hbar^{-1}\langle\hat{\psi}(1)\hat{\psi}^{\dagger}(2)\rangle \\ G^{<}(1,2) &= +i\hbar^{-1}\langle\hat{\psi}^{\dagger}(2)\hat{\psi}(1)\rangle \\ G^{\mathrm{R}}(1,2) &= \theta(t_1 - t_2)[G^{>}(1,2) - G^{<}(1,2)] \\ G^{\mathrm{A}}(1,2) &= \theta(t_2 - t_1)[G^{<}(1,2) - G^{>}(1,2)] \end{aligned} \tag{1}$$

The abbreviation $1 \equiv (\mathbf{r_1}, t_1)$ is used, $\langle \ldots \rangle$ is the statistical average with respect to the density operator, $\theta(t)$ is the unit

978-1-4244-2540-2/08/$25.00 ©2008 IEEE

step function, $\hat{\psi}^\dagger(\mathbf{r_1}, t_1)$ and $\hat{\psi}(\mathbf{r_1}, t_1)$ are the field operators creating or destroying a particle at point $(\mathbf{r_1}, t_1)$ in space-time, respectively. The Green's functions are all correlation functions. For example, $G^>$ relates the field operator $\hat{\psi}$ of the particle at point $(\mathbf{r_1}, t_1)$ in space-time to the conjugate field operator $\hat{\psi}^\dagger$ at another point $(\mathbf{r_2}, t_2)$.

Under steady state condition the Green's functions depend only on time differences. One usually Fourier transforms the time difference coordinate, $\tau = t_1 - t_2$, to energy. For example, the lesser Green's function is transformed as $G^<(1,2) \equiv G^<(\mathbf{r_1}, \mathbf{r_2}; E) = \int (d\tau/\hbar) e^{iE\tau/\hbar} G^<(\mathbf{r_1}, \mathbf{r_2}; \tau)$.

Under steady-state condition the equation of motion for the Green's functions can be written as [23]:

$$[E - H]\, G^{\mathrm{R,A}}(1,2) - \int d3\ \Sigma^{\mathrm{R,A}}(1,3) G^{\mathrm{R,A}}(3,2) = \delta_{1,2} \tag{2}$$

$$G^{\lessgtr}(1,2) = \int d3 \int d4\ G^{\mathrm{R}}(1,3) \Sigma^{\lessgtr}(3,4) G^{\mathrm{A}}(4,2) \tag{3}$$

where H is the single-particle Hamiltonian operator, and Σ^{R}, $\Sigma^<$, and $\Sigma^>$ are the retarded, lesser, and greater self-energies, respectively.

III. Implementation

This section describes the implementation of the outlined NEGF formalism for the numerical analysis of CNT-FETs. A tight-binding Hamiltonian is used to describe the transport phenomena. The self-energy due to electron-phonon interactions are studied next.

A. Tight-Binding Hamiltonian

In Graphene three σ bonds hybridize in an sp^2 configuration, whereas the other $2p_z$ orbital, which is perpendicular to the graphene layer, forms π covalent bonds. The π energy bands are predominantly determining the solid state properties of graphene. Similar considerations hold for CNTs. We use a nearest-neighbor tight-binding π-bond model [24]. Each atom in an sp^2-coordinated CNT has three nearest neighbors, located $a_{\mathrm{cc}} = 1.42$ Å away. The band-structure consists of π-orbitals only, with the hopping parameter $t = V_{pp\pi} \approx -2.7$ eV and zero on-site potential.

The tight-binding Hamiltonian matrix for a $(n, 0)$ zigzag CNT, shown in Fig. 1-a, can be written as [24]

$$\underline{H} = \begin{pmatrix} \underline{U_1} & \underline{t_1} & & & & \\ \underline{t_1} & \underline{U_2} & \underline{t_2} & & & \\ & \underline{t_2}^\dagger & \underline{U_3} & \underline{t_1} & & \\ & & \underline{t_1} & \underline{U_4} & \underline{t_2}^\dagger & \\ & & & \underline{t_2} & \underline{U_5} & . \\ & & & & . & . \end{pmatrix} \tag{4}$$

where the underlined quantities denote matrices. We assume that the electrostatic potential shifts the on-site potential. Therefore, $\underline{U_i}$ is a diagonal matrix which represents the electrostatic potential energy in the ith circumferential ring of carbon atoms. Equal electrostatic potential for all carbon atoms within a ring is assumed, therefore $\underline{U_i} = U_i \underline{I}$. The first and second kind of interaction matrix between the neighboring rings are denoted by $\underline{t_1}$ and $\underline{t_2}$. Only the nearest neighbor interaction between carbon atoms is considered. The coupling matrix between Layer 2 and Layer 3 is diagonal, $\underline{t_1} = t\,\underline{I}$, where t is the hopping parameter. However, the coupling matrix between Layer 1 and Layer 2 is given by

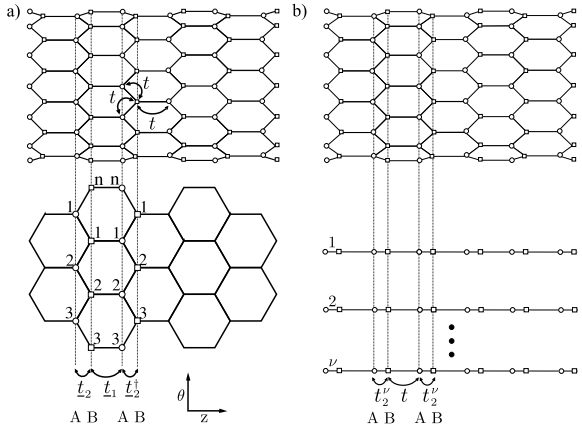

Fig. 1. Layer layout of a $(n, 0)$ zigzag CNT. a) The coupling matrices between layers are denoted by $\underline{t_1}$ and $\underline{t_2}$, where $\underline{t_1}$ is a diagonal matrix and $\underline{t_2}$ includes off-diagonal elements. b) The corresponding one-dimensional chain in mode space with two sites per unit cell with hopping parameters t and $t_2^\nu = 2t\cos(\pi\nu/n)$.

$$\underline{t_2} = \begin{pmatrix} t & & & t \\ t & t & & \\ & t & t & \\ & & . & . \end{pmatrix} \tag{5}$$

The eigenvectors of the matrix $\underline{t_2}$ represent plane waves around the circumference of the CNT with the quantized wave-vectors $k_\nu = 2\pi\nu/\sqrt{3}a_{\mathrm{cc}}n$, where $\nu = 1, 2, \ldots n$ [24], and the eigenvalues $2t\cos(\pi\nu/n)$. By transforming from real space into eigenmode space [25], the subbands become decoupled and the Hamiltonian can be written as $\underline{H} = \sum_\nu \underline{H}^\nu$, where $\underline{H}^\nu$, the Hamiltonian of the subband ν, is given by

$$\mathbf{H}^\nu = \begin{pmatrix} U_1^\nu & t_1^\nu & & & & \\ t_1^\nu & U_2^\nu & t_2^\nu & & & \\ & t_2^\nu & U_3^\nu & t_1^\nu & & \\ & & t_1^\nu & U_4^\nu & t_2^\nu & \\ & & & t_2^\nu & U_5^\nu & . \\ & & & & . & . \end{pmatrix}, \tag{6}$$

with $U_i^\nu = U_i$, $t_1^\nu = t$, and $t_2^\nu = 2t\cos(\pi\nu/n)$ [16, 24]. The one-dimensional tight-binding Hamiltonian $\underline{H}^\nu$ describes a chain with two sites per unit cell with on-site potential U_i^ν and hopping parameters t and t_2^ν, see Fig. 1-b.

B. Electron-Photon Self-Energies

The Hamiltonian of the electron-photon interaction can be written as [26, 27]:

$$\hat{H}_{e-ph} = \sum_{l,m} M_{l,m} \left(\hat{b} e^{-i\omega t} + \hat{b}^\dagger e^{+i\omega t} \right) \hat{a}_l^\dagger \hat{a}_m \tag{7}$$

$$M_{l,m} = (z_m - z_l)\, \frac{i\mathrm{e}}{\hbar} \sqrt{\frac{\hbar I_\omega}{2N\omega\epsilon c}} \langle l | \hat{H}_0 | m \rangle \tag{8}$$

where z_m denotes the position of the carbon atom at site m (Fig. 1-a), I_ω is the flux of photons with frequency ω, and N

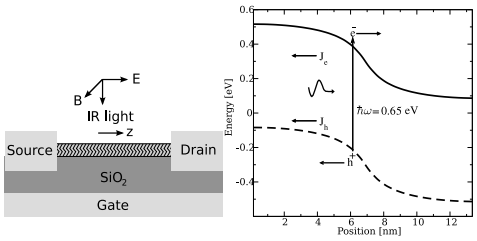

Fig. 2. a) The sketch of the simulated device. b) The process of electron-hole generation by photo-absorption. Incident photons generate electron-hole pairs and the electric field drives electrons and holes towards the drain and source contacts, respectively. $E_{\mathrm{G}} = 0.6$ eV, $\hbar\omega = 0.65$ eV. For the given photon energy the first subband contributes mostly to the total photo-current.

is the photon population number. The incident light is assumed to be monochromatic with polarization along the CNT axis, see Fig. 2. We employed the lowest order self-energy of the electron-photon interaction based on the self-consistent Born approximation [28]:

$$\Sigma^{<,\nu}_{l,m}(E) = \sum_{p,q} M_{l,p} M_{q,m} \times \left[N_\omega G^{<,\nu}_{p,q}(E - \hbar\omega) + (N_\omega + 1) G^{<,\nu}_{p,q}(E + \hbar\omega) \right] \quad (9)$$

The first term corresponds to the excitation of an electron by the absorption of a photon, the second term corresponds to the emission of a photon by de-excitation of an electron.

C. Electron-Phonon Self-Energies

Since in the CNT two degrees of freedom are confined, an electron can only be scattered forward or backward in the axial direction, preserving or changing the sign of the velocity, respectively. We assume bias conditions for which the first subband predominantly contributes to the total current and only intra-subband intra-valley transitions have to be considered. The intraband processes are important for the electrical and heat transport and for relaxation of an excited carrier [29]. The inter-valley processes are possible only for armchair tubes [29].

A linear dispersion relation for acoustic phonons is assumed, $\omega_{q,\lambda} \approx \upsilon_\lambda |q|$, where υ_λ is the acoustic phonon velocity and λ is the phonon polarization. For optical phonons the energy is assumed to be independent of the phonon wavevector $\omega_{q,\lambda} \approx \omega_{\mathrm{OP},\lambda} = \mathrm{const}$. Similarly, the matrix elements of electron-phonon interaction [29] can be approximated as $M_{q,\lambda} \approx M^{\mathrm{AP}}_\lambda |q|$ for acoustic phonons and $M_{q,\lambda} \approx M^{\mathrm{OP}}_\lambda = \mathrm{const}$ for optical phonons. The interaction of electrons with optical phonons is inelastic. Assuming that the electron-phonon interaction occurs locally [30] the lesser self-energy can be written as:

$$\Sigma^{<,\nu}_{\mathrm{inel}}(E) = \sum_\lambda D_{\mathrm{inel},\lambda} \times [N_\lambda G^{<,\nu}(E - \hbar\omega_\lambda) \; + \; (N_\lambda + 1)\, G^{<,\nu}(E + \hbar\omega_\lambda)] \quad (10)$$

N_λ is the phonon occupation number given by the Bose-Einstein distribution function. The electron-phonon interaction strength is determined by

$$D_{\mathrm{inel},\lambda} = \frac{\hbar |M^{\mathrm{OP}}_\lambda|^2}{2 n m_{\mathrm{c}} \omega_\lambda} \quad (11)$$

where m_{c} is the mass of a carbon atom. The first term in (10) corresponds to the emission of a phonon by the de-excitation of an electron, and the second term corresponds to the excitation of an electron by the absorption of a phonon. Interaction with acoustic phonons can be regarded as elastic scattering, $E \pm \hbar\omega_\lambda \approx E$, and the approximation $N_\lambda \approx N_\lambda + 1 \approx k_{\mathrm{B}} T / \hbar \upsilon_\lambda$ can be used. Based on this approximation, the self-energies for acoustic phonon interaction simplify to

$$\Sigma^{\lessgtr,\nu}_{\mathrm{el}}(E) = D^\nu_{\mathrm{el}} G^{\lessgtr,\nu}(E) \quad (12)$$

$$D_{\mathrm{el},\lambda} = \frac{k_{\mathrm{B}} T |M^{\mathrm{AP}}_\lambda|^2}{n m_{\mathrm{c}} \upsilon_\lambda} \quad (13)$$

The self-energy due to electron-phonon interaction comprises the contributions of elastic and inelastic scattering mechanisms, $\Sigma^\nu_{\mathrm{e-ph}} = \Sigma^\nu_{\mathrm{el}} + \Sigma^\nu_{\mathrm{inel}}$.

D. Self-Consistent Simulations

To solve the transport equations numerically they must be discretized in both the spatial and the energy domain. The carrier concentration at some node l of the spatial grid and the current density at the edge between the nodes l and $l+1$ are given by

$$n_l = -4i \sum_\nu \int \frac{dE}{2\pi} G^{<,\nu}_{l,l}(E) \quad (14)$$

$$j_{l,l+1} = \frac{4\mathrm{q}}{\hbar} \sum_\nu \int \frac{dE}{2\pi} 2\Re e\{ G^{<,\nu}_{l,l+1}(E) t^\nu_{l+1,l} \} \quad (15)$$

where the factor 4 is due to the spin and band degeneracy.

For an accurate analysis it is essential to solve the coupled system of transport equations and the Poisson equation self-consistently [20]. The convergence of the self-consistent iteration is a critical issue. To achieve convergence, fine resonances at some energies in (14) have to be resolved accurately. For that purpose an adaptive method for selecting the energy grid is essential [31].

The transport equations must be iterated to achieve convergence of the electron-phonon self-energies, resulting in a self-consistent Born approximation.

IV. The Effect of Electron-Photon Interaction

When scattering via a self-energy is introduced, the determination of the Green's function requires inversion of a matrix of huge rank. To reduce the computational cost, the *local scattering approximation* is frequently used [28, 30, 32, 33]. In this approximation the scattering self-energy terms are diagonal in coordinate representation. This allows to employ the recursive algorithm for computing the Green's functions [12, 28]. The local approximation is well justified for electron-phonon scattering caused by deformation potential interaction [33]. However, we show that this approximation is not justified for electron-photon interaction.

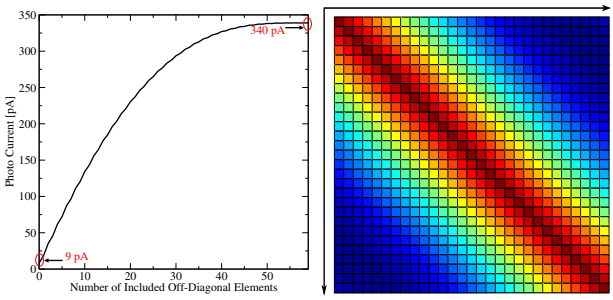

Fig. 3. a) The calculated photo-current as a function of the included off-diagonal elements of the retarded self-energy (Σ^{R}). The current is normalized to the value with full matrix elements. The full matrix size is 60×60. b) The retarded Green's function in two coordinate representation. The existence of relatively large off-diagonal elements indicate the non-locality of the interaction and the need to include the full matrix.

For the given structure (Fig. 2) the calculated photo current is shown in Fig. 3-a. The results are given as a function of the number of included off-diagonal elements of the retarded self-energy, which includes the effects of electron-photon interaction. By including only the diagonal elements of the self-energy (local scattering approximation) the calculated current is only four percent of its correct value. This behavior can be well understood by considering that the electron-photon self-energy is in general non-local and depends on neighboring Green's functions. The off-diagonal elements of the Green's function describe the correlation between different sites. Due to the wave-like behavior of electrons the correlation between neighboring sites is in the order of the electron-wave length. Fig. 3-b shows the Green's function in two coordinate representation. Off-diagonal elements are relatively large, which indicates the need for a full matrix description.

Fig. 4 shows the quantum efficiency of the CNT as a function of the incident photon energy. The efficiency is maximized, when the photon energy matches the band-gap of the CNT; however, at this energy the inclusion of off-diagonal elements becomes more important. This can be understood by considering the fact that at that peak the carrier energy

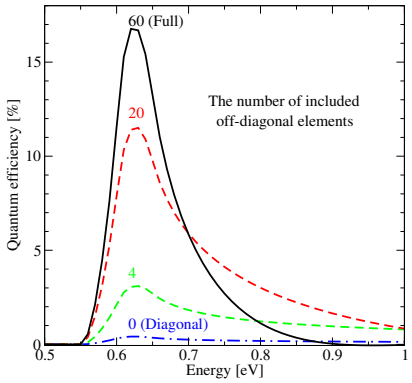

Fig. 4. The quantum efficiency of the CNT as a function of the incident photon energy. The number of included off-diagonal elements of the self-energy has a strong influence on the calculated quantum efficiency.

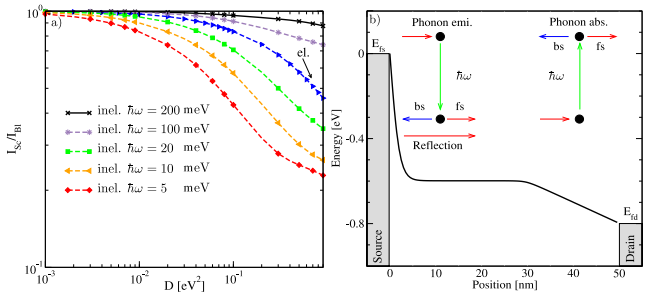

Fig. 5. a) Ballisticity versus electron-phonon coupling strength for a CNT with 50 nm length. Results for both elastic and inelastic scattering with different phonon energies are shown. The operating point is $V_{\mathrm{G}} = V_{\mathrm{D}} = 1$ V. b) Sketch of phonon emission and absorption processes in the channel.

is close to the conduction and valence band energy, where it has a longer wave-length. The result is in agreement with experimental data where the maximum quantum efficiency is estimated to be between 10-20 percent [11].

V. The Effect of Electron-Phonon Interaction

The electron-phonon coupling strength and the phonon energy depend on the chirality and the diameter of the CNT [29]. In this section the device response is studied for a wide range of electron-phonon interaction parameters.

A. Electron-Phonon Coupling Strength

Fig. 5-a shows the ballisticity as a function of the electron-phonon coupling strength. The ballisticity is defined as $I_{\mathrm{Sc}}/I_{\mathrm{Bl}}$, the ratio of the on-current in the presence of electron-phonon interaction to the current in the ballistic case [34].

The left part of Fig. 5-b illustrates an electron losing its kinetic energy by emitting a phonon. The electron will be scattered either forward or backward. In the case of backward scattering the electron faces a thick barrier near the source contact and will be reflected with high probability, such that its momentum will again be directed towards the drain contact.

Elastic scattering conserves the energy of carriers, but the current decreases due to elastic back-scattering of carriers. Fig. 6-a shows that for elastic scattering the source and

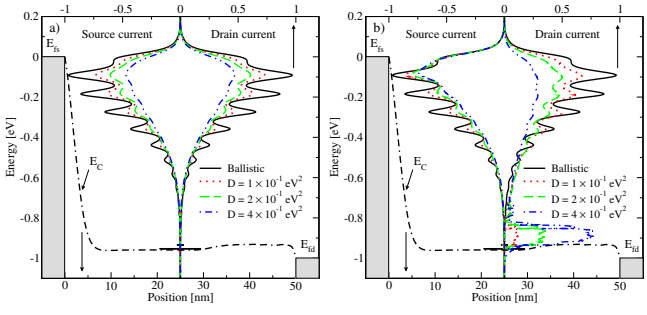

Fig. 6. The spectra of the source and drain currents. a) The effect of elastic phonon scattering with different coupling strengths is shown. b) The effect of inelastic phonon scattering with different coupling strengths is shown. The phonon energy is $\hbar\omega = 100$ meV.

drain current spectra are symmetric. As the electron-phonon coupling strength increases, resonances in the current spectrum are washed out and the total current decreases due to elastic back-scattering. In the case of inelastic scattering, carriers acquiring enough kinetic energy can emit a phonon and scatter into lower energy states. Therefore, as shown in Fig. 6-b, the source and drain current spectra are not symmetric. As the coupling strength increases more electrons are scattered into lower energy states.

B. Phonon Energy

Figure 7-a shows the dependence of the ballisticity with respect to the phonon energy. With increasing phonon energy the effect of phonon scattering on the current is reduced, because scattered electrons lose more kinetic energy and the probability for traveling back to the source contact decreases. The considerable decrease of ballisticity for low energy phonons is due to the phonon absorption process. The right part of Fig. 5-b shows an electron absorbing energy from a phonon and scattering into a higher energy state. In this case the probability for arriving at the source contact increases. This process can severely reduce the total current.

Fig. 7-b separately shows the effects of the phonon emission and absorption processes on the ballisticity. As the phonon energy decreases, the phonon occupation number increases exponentially, and the self-energy contributions of these two components increase. However, due to the higher probability for back-scattering of electrons in the case of phonon absorption, this component reduces the total current more effectively than the phonon emission process.

C. Switching Response

To illustrate the effect of electron-phonon interaction on the dynamic response of the device, the gate-delay time defined as $\tau = (Q_{\rm on} - Q_{\rm off})/I_{\rm on}$ [35] is considered, where the quasi-static approximation is assumed. It has been shown that the quasi-static approximation for CNT based transistors is justified for frequencies below THz [36].

Fig. 8-a shows the ratio of the gate-delay time in the ballistic case to that in the presence of electron-phonon interaction, $\tau_{\rm Bl}/\tau_{\rm Sc}$, as a function of the electron-phonon coupling strength. As the phonon energy increases the gate-delay time increases. This behavior can be attributed to the average electron velocity in the channel, which is high for ballistic electrons and low for electrons scattered to lower energy states.

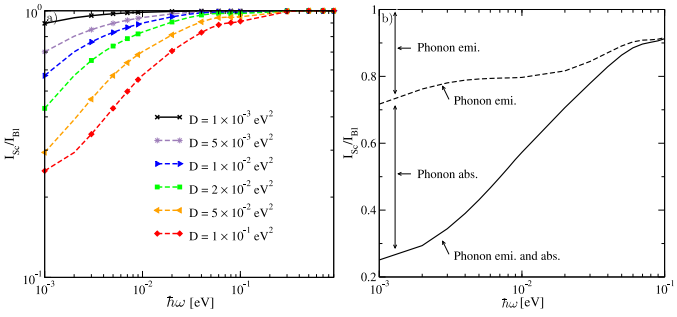

Fig. 7. a) Ballisticity versus phonon energy for a CNT with 50 nm length. Results for inelastic scattering with different electron-phonon couplings are shown. $V_{\rm G} = V_{\rm D} = 1$ V. b) Ballisticity versus phonon energy with $D = 10^{-1}$ eV^2 at the bias point $V_{\rm G} = V_{\rm D} = 1$ V. The contributions due to phonon absorption and emission are shown.

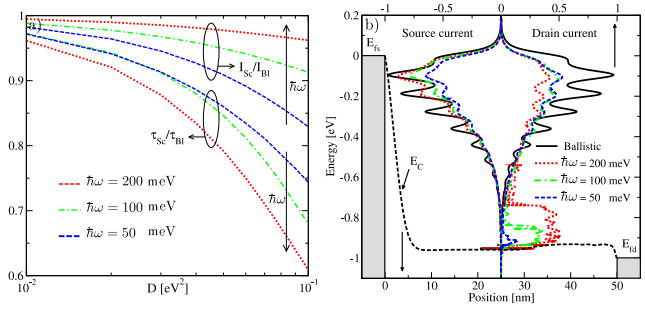

Fig. 8. a) The ratio of the gate-delay time in the ballistic case to that in the presence of electron-phonon interaction. For comparison, the ratio $I_{\rm Sc}/I_{\rm Bl}$ is also shown. b) The spectra of the source and drain currents. The effect of inelastic scattering with different phonon energies is shown. The electron-phonon coupling strength is $D = 2 \times 10^{-1}$ eV^2. A considerable increase of the electron population close to the conduction band-edge as the phonon energy increases is visible.

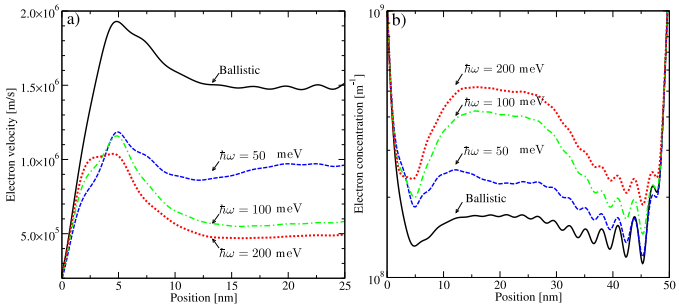

Fig. 9. a) The profile of the electron velocity near the source contact. b) The profile of the electron concentration along the device. The results for the ballistic case and for electron-phonon interaction are shown. As the phonon energy increases the electrons scatter to lower energy states. Therefore, the electron velocity decreases and the carrier concentration increases. The electron-phonon coupling strength is $D = 10^{-1}$ eV^2 and the bias point is $V_{\rm G} = V_{\rm D} = 1$ V.

Fig. 8-b shows the spectra of the source and drain currents for different inelastic phonon energies. Electrons can emit a single phonon or a couple of phonons to reach lower energy states. The probability of multiple phonon emissions decreases as the number of interactions increases. Therefore, as the phonon energy increases, the occupation of electrons at lower energy states increases.

As shown in Fig. 8-b, the electron population close to the conduction band-edge considerably increases as the phonon energy increases. Therefore, as the phonon energy increases the mean velocity of electrons decreases and the carrier concentration in the channel increases (Fig. 9). The increased charge in the channel results in an increased gate-delay time.

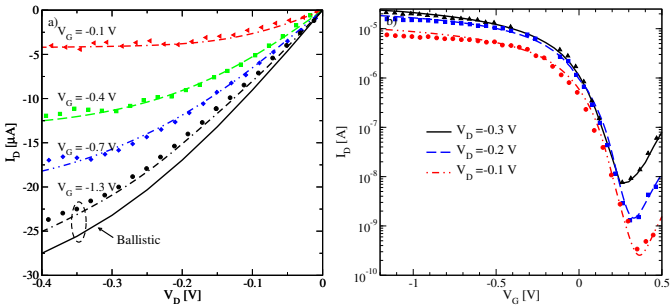

Fig. 10. Comparison of the simulation results and experimental data for the a) output and b) transfer characteristics. Lines show the simulation results and symbols show experimental data. The result for $V_{\rm G} = -1.3$ V is compared with the ballistic limit. Experimental data have been adopted from [37].

VI. Discussion

In general the electron-phonon interaction parameters depend on the diameter and the chirality of the CNT [29]. CNTs with a diameter $d_{\rm CNT} > 2$ nm have a band gap $E_{\rm G} < 0.4$ eV, which render them unsuitable as channel for transistors. Since the fabrication of devices with a diameter $d_{\rm CNT} < 1$ nm is very difficult, we concentrate our study on zigzag CNTs with diameters in the range of $d_{\rm CNT} = 1 - 2$ nm.

Scattering with acoustic phonons is treated as an elastic process. The electron-phonon coupling is also weak for acoustic phonons ($D_{\rm AP} < 10^{-3}$ eV^2), which implies that elastic back-scattering of carriers is weak. Inelastic scattering is induced by optical (OP), radial breathing mode (RBM), and K-point phonons [9, 38]. Considering the class of CNTs discussed, energies of these phonons are $\hbar\omega_{\rm OP} \approx 200$ meV, $\hbar\omega_{\rm RBM} \approx 25$ meV, $\hbar\omega_{\rm K_1} \approx 160$ meV, and $\hbar\omega_{\rm K_2} \approx 180$ meV [34, 38]. The corresponding coupling coefficients are $D_{\rm OP} \approx 40 \times 10^{-3}$ eV^2, $D_{\rm RBM} \approx 10^{-3}$ eV^2, $D_{\rm K_1} \approx 10^{-4}$ eV^2, and $D_{\rm K_2} \approx 10^{-3}$ eV^2 [34].

As discussed in Section V-B, high energy phonons such as OP and K-point phonons reduce the on-current only weakly, but can increase the gate-delay time considerably due to charge pileup in the channel. Low energy phonons such as the RBM phonon can reduce the on-current more effectively, but have a weaker effect on the gate-delay time. However, due to strong coupling, scattering processes are mostly due to electron-phonon interaction with high energy phonons. Therefore, at room temperature the on-current of short CNT-FETs can be close to the ballistic limit [37] (see Fig. 10), whereas the gate-delay time can be significantly below that limit [39, 40].

The intrinsic (without parasitic capacitances) gate-delay time for the ballistic case can be approximated as $\tau \approx 1.7$ ps/μm, or equivalently $f_T \approx 100$ GHz/μm [35]. The highest reported intrinsic cutoff frequency for a device with a length of 300 nm is $f_T \approx 30$ GHz [41], which is far below the ballistic limit. Inelastic electron-phonon interaction with high energy phonons has to be considered to explain the results.

VII. Conclusion

For rigorously modeling current transport in CNT-FETs the coupled system of transport equations and the Poisson equation must be solved self-consistently. A tight-binding Hamiltonian is used to describe the transport phenomena in CNT-FETs. Employing the described model, both the electron-photon and electron-phonon interactions in CNT-FETs can be investigated. The results show that the local scattering approximation, which is widely used in quantum transport simulations, fails to predict the behavior of devices where electron-photon interaction is present. For accurate simulations a non-local self-energy must be taken into consideration. The effect of electron-phonon interaction on the device characteristics is discussed in detail. In agreement with experimental data, the results indicate that at room temperature electron phonon interaction affects the steady-state current of CNT-FETs only weakly, whereas the switching response of such devices can be significantly affected.

Acknowledgment

This work was supported by funds from the Austrian Science Foundation (FWF), contract I79-N16.

References

[1] R. Saito *et al.*, Phys. Rev. B **57**, 4145 (1998).
[2] R. Martel *et al.*, Appl. Phys. Lett. **73**, 2447 (1998).
[3] W. Hoenlein *et al.*, IEEE Trans. Comp. Packag. Technol. **27**, 629 (2004).
[4] J. Appenzeller, Proc. IEEE **96**, 201 (2008).
[5] P. Avouris *et al.*, Nature Nanotechnology **2**, 605 (2007).
[6] A. Javey *et al.*, Nature (London) **424**, 654 (2003).
[7] R. V. Seidel *et al.*, Nano Lett. **5**, 147 (2005).
[8] J.-Y. Park, Nanotechnology **18**, 095202 (2007).
[9] R. Saito *et al.*, *Physical Properties of Carbon Nanotubes* (Imperial College Press, London, 1998).
[10] M. Freitag *et al.*, Phys. Rev. Lett. **93**, 076803 (2004).
[11] M. Freitag *et al.*, Nano Lett. **3**, 1067 (2003).
[12] A. Svizhenko *et al.*, J. Appl. Phys. **91**, 2343 (2002).
[13] J. Guo, J. Appl. Phys. **98**, 063519 (2005).
[14] J. Guo *et al.*, IEEE Trans. Nanotechnol. **4**, 715 (2005).
[15] A. Svizhenko *et al.*, IEEE Trans. Nanotechnol. **4**, 557 (2005).
[16] A. Svizhenko *et al.*, Phys. Rev. B **72**, 085430 (2005).
[17] M. Pourfath *et al.*, Nanotechnology **18**, 424036 (2007).
[18] W. Tian *et al.*, J. Chem. Phys **109**, 2874 (1998).
[19] Y. Xue *et al.*, Phys. Rev. B **69**, 085403 (2004).
[20] A. W. Ghosh *et al.*, Nano Lett. **4**, 565 (2004).
[21] L. P. Kadanoff *et al.*, *Quantum Statistical Mechanics: Green's Function Methods in Equilibrium and Non-Equilibrium Problems* (W.A. Benjamin, New York, 1962).
[22] G. D. Mahan, *Many-Particle Physics*, *Physics of Solids and Liquids*, 2nd ed. (Plenum Press, New York, 1990).
[23] S. Datta, *Electronic Transport in Mesoscopic Systems* (Cambridge University Press, New York, 1995).
[24] J. Guo *et al.*, Intl. J. Multiscale Comput. Eng. **2**, 257 (2004).
[25] R. Venugopal *et al.*, J. Appl. Phys. **92**, 3730 (2002).
[26] E. Lindor *et al.*, J. Appl. Phys. **91**, 6273 (2002).
[27] D. A. Stewart *et al.*, Phys. Rev. Lett. **93**, 107401 (2004).
[28] R. Lake *et al.*, J. Appl. Phys. **81**, 7845 (1997).
[29] V. N. Popov *et al.*, Phys. Rev. B **74**, 075415 (2006).
[30] R. Lake *et al.*, Phys. Rev. B **45**, 6670 (1992).
[31] M. Pourfath *et al.*, J. Comp. Electronics **5**, 155 (2006).
[32] S. Datta, J. Phys.:Condensed Matter **2**, 8023 (1990).
[33] S. O. Koswatta *et al.*, IEEE Trans. Electron Devices **54**, 2339 (2007).
[34] S. O. Koswatta *et al.*, Appl. Phys. Lett. **89**, 023125 (2006).
[35] Y. Yoon *et al.*, IEEE Trans. Electron Devices **53**, 2467 (2006).
[36] Y. Chen *et al.*, Appl. Phys. Lett. **89**, 203122 (2006).
[37] A. Javey *et al.*, Nano Lett. **4**, 1319 (2004).
[38] J. Park *et al.*, Nano Lett. **4**, 517 (2004).
[39] D. Frank *et al.*, IEEE Electron Device Lett. **25**, 34 (2004).
[40] X. Huo *et al.*, in *Intl. Electron Device Meet. Tech. Dig.* 691 (2004)
[41] A. L. Louarn *et al.*, Appl. Phys. Lett. **90**, 233108 (2007).